Scanning tunneling microscopy and spectroscopy of NaCl overlayers on the stepped Cu(311) surface: Experimental and theoretical study

F. E. Olsson and M. Persson
Department of Applied Physics, Chalmers/Göteborg University, S-41296 Göteborg, Sweden

J. Repp and G. Meyer
IBM Research, Zurich Research Laboratory, CH-8803 Rüschlikon, Switzerland
(Received 11 March 2004; revised manuscript received 11 November 2004; published 24 February 2005)

The physical properties of ultrathin NaCl overlayers on the stepped Cu(311) surface have been characterized using scanning tunneling microscopy (STM) and spectroscopy, and density-functional calculations. Simulations of STM images and differential conductance spectra were based on the Tersoff-Hamann approximation for tunneling with corrections for the modified tunneling barrier at larger voltages and calculated Kohn-Sham states. Characteristic features observed in the STM images can be directly related to calculated electronic and geometric properties of the overlayers. The measured apparent barrier heights for the mono-, bi-, and trilayers of NaCl and the corresponding adsorption-induced changes in the work function, as obtained from the distance dependence of the tunneling current, are well reproduced and explained by the calculated results. The measurements revealed a large reduction of the tunneling conductance in a large voltage range, resembling a band gap. However, the simulated spectrum showed that only the onset at positive sample voltages may be viewed as a valence-band edge, whereas the onset at negative voltages is caused by the drastic effect of the electric field from the tip on the tunneling barrier.

DOI: 10.1103/PhysRevB.71.075419 PACS number(s): 68.35.Ct, 68.55.Ac, 68.37.Ef

I. INTRODUCTION

Thin films of insulating materials on metal surfaces are of direct technological interest in microelectronics, catalysis, and as a corrosive protection. They also attract increasing interest in nanoscience and nanotechnology as potential substrates for atomic and molecular manipulation by the scanning tunneling microscope (STM). In particular, this interest stems from the small electronic interaction of assembled molecules and adatoms with the metal support. The nonvanishing electron density that extends through the ultrathin (thickness below 1 nm) insulating films allows STM studies of these surfaces.[1–3] A prerequisite for the realization of this is the ability to grow stable and atomically thin insulating films on metal surfaces with a well-characterized and ordered geometric structure. So far the number of systems studied that fulfill these conditions has been very limited.[4] An interesting model system is provided by NaCl overlayers on a stepped Cu(311) surface, which we have studied in detail using STM,[5] and also most recently by density-functional calculations.[6]

These experimental and theoretical studies revealed several interesting aspects of the growth, structure, and bonding of these systems. The initial growth of NaCl on the Cu(311) surface was found to be two dimensional and commensurate. In the experimental study, the lattice match of the overlayer with the substrate was suggested to be stabilized by the incomplete screening of the step Cu atoms resulting in an electrostatic interaction between these atoms and the Cl^- ions. Density-functional calculations corroborated this suggestion and also showed that the bonding of the overlayer on the surface was further stabilized by the formation of a weak chemical bond between the step Cu atoms and the Cl^- ions. In addition, these calculations revealed large relaxations of the monolayers, such as a buckling of the layer with a large influence on the work function. These results call for a detailed STM study of the topography of and the tunneling conductance through these overlayers. In particular, no insulating overlayers on metal surfaces for biases well below 1 V have so far been imaged.

In this paper, we present atomically resolved topographical images of NaCl mono-, bi- and tri-layers on Cu(311) obtained by STM and discuss them in relation to simulated images based on density-functional calculations and the Tersoff-Hamann (TH) approximation.[7] In this approximation, STM images and scanning tunneling spectra are obtained from the local density of states (LDOS) at the position of the tip apex. The conductivity of the samples is further investigated using scanning tunneling spectroscopy. The measured dI/dV spectra are compared with simulated spectra and discussed in relation to the energy dependence of the calculated LDOS. This study also includes a calculation and discussion of the apparent heights and work functions of these layers obtained from tunneling measurements. The apparent height of an NaCl overlayer contains information about the "local" work function, that is, the tunneling barrier. The tunneling barriers are obtained from the measured distance dependence of the tunneling conductance.

STM investigations of insulating overlayers provide important information about the growth mechanisms and the local electronic structure of the overlayer. In earlier STM investigations of ultrathin insulating overlayers on metal surfaces, such as MgO on Ag(100),[2] and NaCl on Al(111) and Al(100),[1] the experiments were carried out at relatively high biases of about 1 eV to provide atomic resolution of the overlayer. Atomically resolved STM images have also been

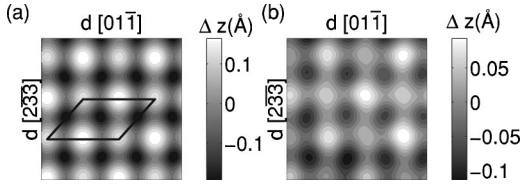

FIG. 1. Experimental STM images and calculated LDOS images of a NaCl monolayer in the $p(3\times2)$-II structure. (a) Calculated LDOS image at an average distance of 7.9 Å from the Cu(311) surface. The surface unit cell used in the calculation, see Fig. 4 (right), is indicated. (b) Experimental STM image with tunneling parameters 210 pA and −24 meV. In (a) and (b) the area shown is 15×15 Å^2.

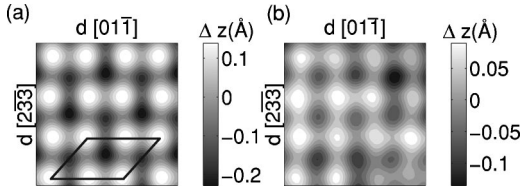

FIG. 2. Experimental STM images and calculated LDOS images of a NaCl monolayer in the $p(3\times2)$-I structure. (a) Calculated LDOS image at an average distance from the Cu(311) surface of 7.9 Å. The surface unit cell used in the calculation, see Fig. 4 (left), is indicated. (b) Experimental STM image with tunneling parameters 210 pA and 24 meV. In (a) and (b) the area shown is 15×15 Å^2.

obtained for NaCl layers on Ge(100),[8] in which only one type of ions was found to be imaged as a protrusion.[1] A combined STM and density-functional study of NaCl layers on an Al(111) and Al(100) surface revealed that only the Cl^- ions were imaged as protrusions. In this work, the atomic contrast as well as the apparent height of the NaCl layers was discussed by comparing the experimental images with calculations of LDOS within the TH approximation. MgO layers on an Ag(100) surface were studied using measured dI/dV spectroscopy, and the band gap of the bulk MgO electronic structure was found to be developed within the first three monolayers.[2] This finding was corroborated by density-functional calculations of the energy dependence of the LDOS within the MgO layers.

The paper is organized as follows. In Sec. II our experimental STM and dI/dV results for mono-, bi-, and trilayers of NaCl on Cu(311) are presented. In Sec. III we present the geometric and electronic structure, simulated STM images, and dI/dV spectra for the same systems. The experimental and theoretical results are compared and discussed in Sec. IV. Finally, Sec. V concludes the paper.

II. EXPERIMENTAL METHODS AND RESULTS

Our experiments were carried out with a low-temperature STM,[9] operated at 13 K. We used a chemomechanically polished Cu(311) single crystal, which was cleaned by Ne^+ sputtering and annealing at 750 K. NaCl was evaporated thermally, and the deposition and annealing temperature was varied in the range of 400-570 K. In this temperature range Cu surface atoms are mobile. We used an electrochemically etched tungsten wire as STM tip. Bias voltages refer to the sample voltage with respect to the tip. The STM images were taken at 13 K. The STM images for mono- and bilayers that are presented in Figs. 1(b), 2(b), and 3(b) and for bare Cu(311) were acquired at relatively low voltages of $|V| \leqslant 100$ mV, that is, well within the band gap of bulk NaCl. For the bare Cu(311) and the monolayer structures our experimental images were obtained under identical tunneling conditions, that is, applied current and voltage, as well as the tip were identical. Because the growth of the first layer is always completed before the formation of the second layer we could not be sure that the tip structure was identical in the imaging of the bare and the bilayer covered surfaces as in the case of the bare and monolayer-covered surfaces. However, we were able to record STM images of islands of mono-, bi-, and trilayers simultaneously. Up to four layers of NaCl could be imaged with atomic resolution.

In our experiments we observe two different structures for the NaCl monolayer, shown in Figs. 1(b) and 2(b). As suggested in our earlier study,[5] we attribute these images to be associated with the structures presented in Fig. 4. Here we follow the notation of Ref. 6 and designate these structures as $p(3\times2)$-II and $p(3\times2)$-I, respectively.[10] In the STM images of these structures, we identify one characteristic feature for each structure. In the STM image of the $p(3\times2)$-II structure every second protrusion appear slightly brighter. For the $p(3\times2)$-I structure we note a slight tendency for the protrusions to group into pairs, even though this effect is small and at the limit of the experimental resolution. In contrast to the monolayer, atomically resolved STM images of the bi- and trilayers [Fig. 3(b)] did not show any differences between the domains corresponding to $p(3\times2)$-I and -II structures, although it could be concluded that both domains are present with the help of characteristic defects consisting of a missing Cu atoms in the topmost substrate layer.[5]

The apparent heights Δz_l of the NaCl overlayers ($l=1$, 2, 3 for the mono-, bi-, and trilayer) are presented in Table I.

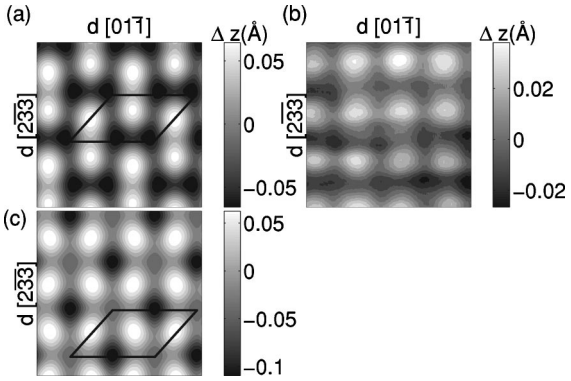

FIG. 3. Experimental STM image and calculated LDOS images of NaCl bilayer structures on Cu(311). (a) and (c) Calculated LDOS image for the $p(3\times2)$-I and $p(3\times2)$-II structures, respectively, at an average distance of 9.0 Å from the Cu(311) surface. The surface unit cells used in the calculations, see Fig. 4, are indicated. (b) Experimental STM image of the $p(3\times2)$-I bilayer structure with tunneling parameters 360 pA and 100 meV. The STM images of the $p(3\times2)$-I and $p(3\times2)$-II structures could not be discriminated. In (a), (b), and (c) the area shown is 15×15 Å^2.

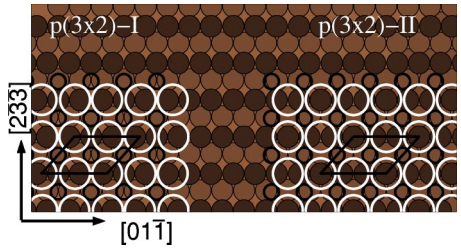

FIG. 4. Ordered structures of a NaCl monolayer on Cu(311): (left) $p(3\times2)$-I and (right) $p(3\times2)$-II. The dark and light filled circles represent Cu atoms of the first and second layer, respectively, and the large white and small black open circles represent Cl^- and Na^+ ions, respectively. The unit cells used in the calculations are indicated. In the $p(3\times2)$-I structure, all Cl^- ions sites are equivalent, whereas there are two inequivalent Na^+ ion sites. In the $p(3\times2)$-II structure, all Na^+ ion sites are equivalent, whereas there are two inequivalent Cl^- ions sites; see also Fig. 1 in Ref. 6.

Δz_l is defined as the vertical change in tip position when a step edge is scanned. We find that Δz_l decreases with l and is positive for all l. As also shown in Table I, the geometric heights $\Delta z_l^{\mathrm{geom}}$ of the NaCl overlayers are about 1 Å larger than Δz_l. This implies that the tip-surface distance decreases with l.

To quantify work-function changes upon adsorption of NaCl layers, we carried out measurements of the distance dependence of the tunneling current I.[11] The feedback loop was switched off and a voltage ramp was applied to the z-piezo drive while measuring the current I as a function of the tip-sample distance z. The sweep in z measured 2.7 Å in height and had a duration of about 1 sec. The resulting current curve closely followed an exponential dependence, $I(z)\propto\exp(-2\kappa z)$, from which an apparent barrier height $\overline{\Phi}$ was determined from the decay constant κ as $\overline{\Phi}=\hbar^2\kappa^2/(2m_e)$. The relationship between $\overline{\Phi}$ and the work function Φ of the sample is not straightforward and has been discussed at length in the literature.[12,13] The systematic deviation of $\overline{\Phi}$ from Φ decreases with increasing tip-surface distance, corresponding to a larger vacuum region between the tip and the sample. Therefore this deviation was minimized by recording spectra at a very low current, down to 10 pA, so as to maximize the tip-surface distance. Although Φ cannot be determined directly, the adsorption-induced relative changes in $\overline{\Phi}$ are expected to correspond to the relative changes in Φ. The experimental uncertainty in determining $\overline{\Phi}$ from κ is set by the vertical length scale calibration, and is a few percent. Using this procedure, we find that the measured work-function difference between a NaCl monolayer and the clean surface agrees well with the work-function difference measured by an atomic force microscopy tip.[14]

The apparent barrier heights $\overline{\Phi}$ for the bare surface and NaCl overlayers deduced from the measured $I(z)$ are shown in Table I. These results show that there is a substantial decrease in $\overline{\Phi}$ upon adsorption of the first layer and an even larger decrease for the second layer. No further changes of $\overline{\Phi}$ are observed for the thicker layers. This indicates that the nature of the monolayer differs from that of the interface layer in the multilayers.

The insulating properties of the monolayer have been investigated using dI/dV spectroscopy, as shown in Fig. 5. The distances used when acquiring spectra are about 6 Å larger than the distance for the imaging. The spectra are not sensitive to the tip position relative to the surface. The poor conductivity of the monolayer is manifested by a very small tunneling current between -4 and $+3$V and exponential off and onsets of dI/dV at these voltages. The other characteristic feature in the spectra is the shoulder at about $+3.2$ V.

III. THEORETICAL METHODS AND RESULTS

The results obtained from the STM measurements for the bare surface and the NaCl overlayers, such as constant current images, work functions, and apparent heights, have been analyzed by extending our recent density-functional calculations of the electronic and geometric structures of these system,[6] now including also the trilayer, to tunneling. These calculations were based on a plane-wave basis set and the projector augmented wave (PAW) method[15,16] as implemented in the VASP (Ref. 17) code. A generalized gradient approximation[18] was employed for the exchange-correlation potential. The system was represented by a slab in a supercell geometry with NaCl overlayer on one side of the slab[19] and the equilibrium geometry was obtained by a structural optimization.[20] The electric dipole field from the asymmetric slab was compensated by an external electric dipole field in the vacuum region.[21,22] The work function was obtained from the calculated electrostatic potential in the vacuum region and the Fermi energy (ϵ_F). We considered the two $p(3$

TABLE I. Calculated work function Φ_{theory} and experimentally measured mean barrier height $\overline{\Phi}_{\mathrm{expt.}}$ of NaCl layers on Cu(311). The values in parentheses indicate the relative changes with respect to the clean Cu surface. Δz_l is the apparent height obtained from LDOS calculations (theory) and STM experiments (expt) and $\Delta z_l^{\mathrm{geom}}$ is the calculated geometric height. $l=1$, 2, and 3 for mono-, bi-, and trilayers, respectively. The result for the NaCl monolayer is for the $p(3\times2)$-II structure.

	Cu(311)	mono	bi	tri
Φ_{theory} (eV)	4.31	3.53 (−18%)	3.05 (−30%)	3.24 (−25%)
$\overline{\Phi}_{\mathrm{expt.}}$ (eV)	3.81	3.23 (−15%)	2.82 (−26%)	2.82 (−26%)
Δz_l (expt) (Å)		1.6	1.4	1.3
Δz_l (theory) (Å)		1.8	1.1	
$\Delta z_l^{\mathrm{geom}}$ (Å)		2.5	2.8	2.8

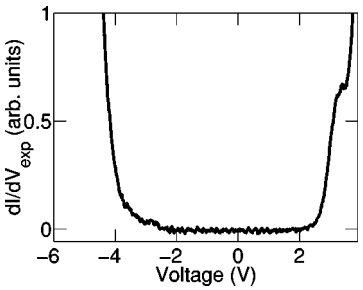

FIG. 5. Experimental dI/dV spectrum for a monolayer NaCl on Cu(311). The tip-sample distance corresponds to a current set point of $I=0.3$ nA at $V=3.8$ V. This distance is about 6 Å larger than the distance for the imaging parameter set used in Figs. 1 and 2.

$\times 2$)-I and $p(3\times 2)$-II structures for the NaCl monolayer, shown in Fig. 4, and the structures for the bilayer were formed by adding one NaCl layer on these monolayer structures. For the trilayer, we only considered the structure that was formed by adding two NaCl layers on the $p(3\times 2)$-I monolayer structure.

In Table I and Fig. 6, we show the calculated work functions and key bonding parameters of the NaCl layers, respectively. For easy reference these tables also include the parameters for monolayer and the $p(3\times 2)$-I bilayer from Ref. 6. The adsorption energy and the geometric structure of the topmost layer for the $p(3\times 2)$-II bilayer structure are basically identical to the corresponding results for the $p(3\times 2)$-I bilayer structure, and are not presented. The geometric structures of the interface layers for the $p(3\times 2)$-I and $p(3\times 2)$-II structures resembles those of the monolayer, although the NaCl buckling is decreased. The calculated *s*, *p*, and *d* partial density of states (PDOS) of the Cl^- ions in the topmost layers of the mono-, bi-, and trilayers are shown in Fig. 7. As expected, the width of the Cl^- peak is largest for the monolayer [Fig. 7(c)] and smallest for the trilayer [Fig. 7(a)], due to larger overlap with the Cu states for the interface layer. Note that electric polarization of the Cl^- ions due to the presence of the Cu substrate only involve minor filling of 4*s* and emptying of 3*p* states and is difficult to identify in the PDOS.

The STM images and the apparent heights of the overlayers were simulated using the TH approximation[7] for the tunneling current in which the tunneling current for low bias is proportional to the LDOS, $\rho(\mathbf{r_0},\epsilon_F)$, of the surface at the position of the tip apex, $\mathbf{r_0}$. The LDOS was calculated from the Kohn-Sham wave functions; see Ref. 23 for details. The topographical STM images were obtained from the topography of the contours of constant $\rho(\mathbf{r_0},\epsilon_F)$, which henceforth will be referred to as LDOS images.

We have also simulated differential conductance dI/dV spectra, using the LDOS outside the surface. For these simulations it is necessary to consider the effects the applied electric field from the tip has on the tunneling. Following Lang,[24] these effects are partly accounted for by calculating dI/dV within the average tunneling barrier approximation as

$$\frac{dI}{dV} \propto \frac{d}{dV}\left(\int_{\epsilon_F}^{\epsilon_F+eV} \rho_S(\epsilon)T(\epsilon,V)d\epsilon\right)$$
$$= e\rho_S(\epsilon_F+eV)T(\epsilon_F+eV,V)$$
$$+\int_{\epsilon_F}^{\epsilon_F+eV}\frac{d}{dV}(\rho_S(\epsilon)T(\epsilon,V))d\epsilon, \qquad (1)$$

where $T(\epsilon,V)$ is the transmission coefficient through the average barrier for an electron with energy ϵ and is given by

$$T(\epsilon,V)=\exp[-2s\sqrt{2m(\Phi_{av}+\epsilon_F-\epsilon+eV/2)}/\hbar]. \qquad (2)$$

Here $\Phi_{av}=(\Phi_T+\Phi_S)/2$ where Φ_T and Φ_S is the tip and sample work function, respectively, $\rho_S(\epsilon)$ is the LDOS at a distance z_s just outside the surface layer defining the boundary of the vacuum region, and *s* is the distance between z_s and the tip apex. The first term in Eq. (1) is the LDOS at the tip apex taking into account electric field in the tunneling junction. In the limit of vanishing voltage only this term survives and the TH approximation is recovered. Note that this result for dI/dV is well defined for $|V|<2\Phi_{av}$ but the average barrier approximation breaks down for voltages approaching the field-emission regime, that is, for $V>\Phi_S/e$ or $V<-\Phi_T/e$.

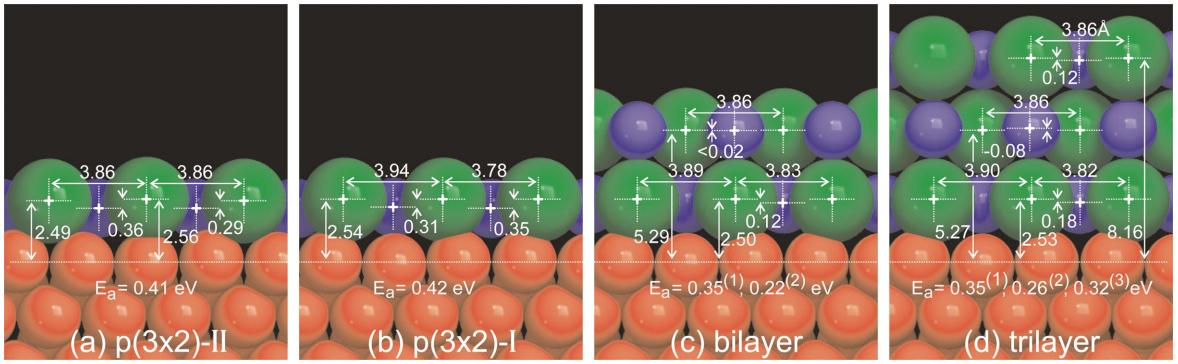

FIG. 6. (Color) Calculated interface energies and geometrical parameters of a NaCl (a) $p(3\times 2)$-II mono-, (b) $p(3\times 2)$-I mono-, (c) $p(3\times 2)$-I bi-, and (d) $p(3\times 2)$-I trilayer on the (311) surface of Cu(311). The small, medium, and large spheres represent Na, Cu, and Cl, respectively. The interface layer for the bi- and trilayer correspond to the $p(3\times 2)$-I structure. The geometrical parameters are given in Å. The adsorption energies E_a are given in eV per NaCl pair and is defined as $E_a=(E_{n\mathrm{NaCl}}+E_{(l-n)\mathrm{NaCl/Cu}}-E_{l\mathrm{NaCl/Cu}})/m$, where *l* is the number of NaCl layers, *m* is the number of NaCl in the interface, and $n=1$, $n=1$, 2, and $n=1$, 2, 3, for mono-, bi-, and trilayers, respectively. *n* is shown as superscipts of E_a for the bi- and trilayers.

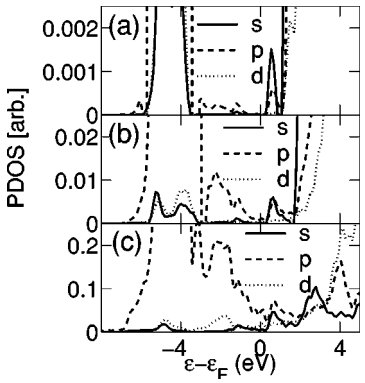

FIG. 7. Partial *s*, *p*, and *d* density of states (PDOS) around the topmost Cl^- ions in a NaCl (a) tri-, (b) bi-, and (c) monoayer on Cu(311). Note that the scales of the partial density of states for the different layers differ by several orders of magnitude.

In Fig. 8, we show the simulated dI/dV spectra for a monolayer of NaCl in the $p(3\times2)$-II structure. The behavior of dI/dV in the voltage region from -3 to 3 V is well understood from the behavior of the LDOS. In particular, the rapid increase of dI/dV around $V=2$ V is an LDOS effect and may be viewed as conduction-band edge. In contrast, the rapid decrease of dI/dV around $V=-4.5$ V is not an LDOS effect associated with any valence-band edge. Note that the large contribution of electron states of *p* or *s* character around the Cl^- ions to the PDOS in Fig. 7 in the corresponding energy region does not show up in the LDOS. As illustrated by the result for dI/dV in Fig. 8, using an energy-independent $\rho_S(\epsilon)=\rho_S(\epsilon_F)$, the rapid decrease stems from the second term in Eq. (1), which describes the drastic effect of the voltage dependent barrier on the tunneling and the larger probability for tunneling of electrons with energies closer to the vacuum level at larger negative voltages. In the calculation we have used the same work function for the tip and the sample, so we expect an even more dramatic onset of dI/dV for $V<-3.5$ V, corresponding to the field-emission regime.

IV. DISCUSSION

We begin by comparing and discussing the measured apparent barrier heights and calculated work functions for the

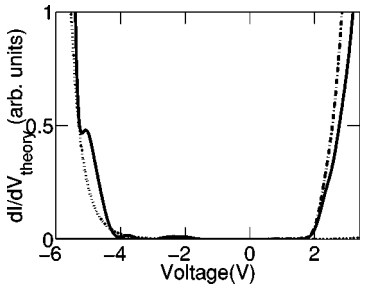

FIG. 8. Calculated dI/dV spectra for a monolayer NaCl in the $p(3\times2)$-I structure on Cu(311). The solid and dotted lines are calculated from Eq. (1) using the full energy dependence of $\rho_S(\epsilon)$ and a constant $\rho_S(\epsilon)$, $\rho_S(\epsilon)=\rho_S(\epsilon_F)$, respectively. The dashed-dotted line is the result obtained using only the LDOS contribution to dI/dV [first term in Eq. (1)]. In the calculations we used $z_s=2$ Å, $s=10$ Å, and $\Phi_{av}=3.5$ eV.

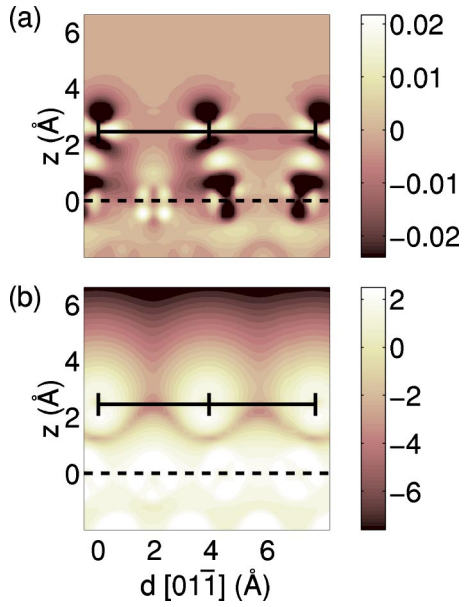

FIG. 9. (a) Electron-density difference, $\Delta\rho$ (electrons/Å^3) and (b) $\ln(\rho(\epsilon_F))$ (arbitrary units) along $[01\bar{1}]$ for the $p(3\times2)$-I monolayer structure. The position of the Cl^-, at $d[01\bar{1}]=0$, 3.94 and 7.71 Å, are indicated. The solid and dashed lines indicate the positions of the Cl^- ions and the Cu surface reference plane, respectively. Both $\Delta\rho$ and $\ln(\rho(\epsilon_F))$ have been truncated.

$p(3\times2)$-I monolayer, the bilayer, and the trilayer. As shown in Table I, the calculated decrease in work functions with increasing layer thickness nicely reproduce the measured decrease. Note that the measured apparent barrier height and the calculated work function cannot be compared directly. From the calculations we are able to understand the reduction of Φ upon adsorption and its layer dependence in terms of bonding and buckling of the monolayer. This explanation was discussed in detail in our previous study[6] and will only be summarized here.

In general, the surface contribution to Φ is determined by the surface dipole layer, to which both electronic and ion-core rearrangements upon adsorption contribute. The reduction of Φ upon adsorption was argued to be due to the formation of a weak chemical bond between the Cl^- ions and the metal substrate, as revealed by the density differences upon adsorption in Fig. 9 (see also Fig. 3 in Ref. 6) and the screening of the Na^+ ion by the metal electrons.

The substantially smaller reduction of Φ for the monolayer than for the bilayer and the trilayer is explained by the large buckling of the monolayer with a large inward relaxation of the Na^+ ions relative to the Cl^- ions, resulting in a dipole layer that increases the work function. This buckling is reduced substantially for the bilayer and the trilayer, and the work-function reductions for these layers are governed mostly by the electronic rearrangements, which are limited to the interface region. The measured Φ is thus consistent with a buckling of the monolayer and an interface bonding that involves electron rearrangements between the overlayer and the substrate.

Next we turn to a comparison and a discussion of observed and simulated STM images for the bare surface and

the overlayers. These images contain information about the surface electronic and geometric structure through the tails of the wave functions in the vacuum region. Because the TH approximation for the tunneling is not based on any detailed model of the tip *s* density of states, we are not able to determine the distance z_0 between the tip apex and the surface Cu layer from the tunneling conductance. However, the bare surface and the two monolayers were imaged under identical tunneling conditions so that we can use the image for the bare surface to calibrate the value of $\rho(\mathbf{r_0}, \epsilon_F)$ in the calculation of the LDOS images and to make a prediction for the images for the monolayers.

For the bare Cu surface, the calculated LDOS image gives the same tip-surface corrugation across the Cu rows as the STM image at an average z_0 of about 6.1 Å. No corrugation could be resolved along the Cu rows either in the LDOS image or in the STM image. In contrast to the flat single-crystal metal surfaces for which the TH approximation fails to reproduce atomically resolved STM images,[25] the measured tip-surface corrugation can be reproduced by a realistic value for z_0, for which the TH approximation should be applicable. For flat metal surfaces, the mechanism behind atomic resolution in imaging has been argued to involve a direct tip-surface interaction.[26]

In Figs. 1 and 2, we show the calculated LDOS images for the monolayers investigated, using the same value of $\rho(\mathbf{r_0}, \epsilon_F)$ as for the bare surface that reproduced the observed surface corrugation. The corresponding average value of z_0 is 7.9 Å. The resulting LDOS images overall are in good agreement with the observed STM images although the corrugation is somewhat larger in the LDOS images than in the STM images. The LDOS images support our original interpretation of the observed STM images, namely, that the protrusions correspond to Cl^- ions.[5] From the dependence of the LDOS at ϵ_F perpendicular to the surface, Fig. 9, we note that the states that extend furthest into the vacuum region and contribute mostly to the tunneling has *s* character, namely, the Cl 4*s* states. As indicated in the PDOS in Fig. 7, there are contributions from *s*, *p*, and *d* states at the Fermi energy, where the *s* states derive from the filling of Cl 4*s* state.

As shown in Fig. 1, the LDOS image for the $p(3\times2)$-II monolayer nicely reproduces the experimental observation that every second Cl appears slightly brighter. In our calculations we attribute the brighter protrusions to Cl^- ions at bridge sites. This difference in brightness corresponds to a difference in z_0 of about 0.05 Å and is consistent with a larger adsorption height z_{Cl} of 0.07 Å (see Fig. 6) for the Cl^- ions at the bridge sites than at the top sites. However, the mixing of the 3*p* Cl states with the metal states at the Fermi level is found to be stronger for the top site than for the bridge site. This electronic effect counteracts in part the geometric effect on the corrugation of the LDOS image.

As shown in Fig. 2, the pairing of the protrusions in the STM image for the $p(3\times2)$-I monolayer is well reproduced by the LDOS image. This pair formation reflects the geometric relaxations of the Cl^- ions along the Cu rows, resulting in two different Cl-Cl distances, which differ by 0.16 Å (see Fig. 6). However, the apparent difference in distance as extracted from the images is significantly larger than the geometric relaxations, about 0.9 Å. In fact, the geometric pairing effect is exaggerated by electronic effects, which are dominated by a better overlap of 4*s* states of two paired Cl^- ions. The pairing shows up in the contour plot of the LDOS at ϵ_F normal to the surface, Fig. 9(b). Note that, the increase in LDOS at ϵ_F between the Cl^- ions that are closer to each other is not reflected in the electron density difference, Fig. 9(a), where the tilting of the Cl 3*p* states due to mixing with Cu states results in a decrease of electron density. This mixing implies an effective increase in Cl 3*p* states at ϵ_F, which is not resolved in the total LDOS at ϵ_F.

In comparing STM and LDOS images of the bilayer, we cannot adopt the same unambiguous procedure for the choice of average z_0 as we used for the monolayers. The bare surface and the bilayer are never imaged under the same tunneling conditions because the monolayer is fully developed before the formation of the bilayer. However, in our comparison with the STM image we use the same value for $\rho(\mathbf{r_0}, \epsilon_F)$ as above, which corresponds to an average z_0 of 9.0 Å. As for the monolayers we find that the protrusions in the LDOS image for both the $p(3\times2)$-I and $p(3\times2)$-II structures of the bilayer shown in Figs. 3(a) and 3(c), respectively, correspond to Cl^- ions. As shown in Fig. 7, also the bilayer has a contribution from Cl states to the partial density of states around the Fermi level. This contribution is much smaller than for the Cl^- ion in the monolayer but is compensated by the average distance of the tip from the outermost NaCl layer of only about 3.5 Å for the bilayer and thus about 2 Å shorter than the corresponding distance for the monolayer with the same value of $\rho(\mathbf{r_0}, \epsilon_F)$. The main difference between the $p(3\times2)$-I and $p(3\times2)$-II bilayer LDOS images is the pairing of the protrusions in the former image. Since the distances between Cl^- ions are the same for the two bilayer structures, this pairing is purely an electronic structure effect. We attribute the pairing tendency of the protrusions to differences in the electronic polarization of the outermost Cl^- ions deriving from differences in the Cl-Cl bond length in the interface layers. In the $p(3\times2)$-II bilayer structure, there is no such bond length differences in the interface layer, whereby there is no pairing in the LDOS image.

The LDOS images for the $p(3\times2)$-I and $p(3\times2)$-II bilayer structures, Figs. 3(a) and 3(c), respectively, can be clearly discriminated from the pairing and nonpairing of the protrusions, respectively. This is in contrast to the STM images for the bilayer stuctures, where there are experimental indications that both bilayer structures exist, although their STM images could not be discriminated, as discussed in Sec. II. A direct comparison of the STM and LDOS images for the bilayer yields a near quantitative agreement for the $p(3\times2)$-II bilayer structure, whereas the agreement is qualitative for the $p(3\times2)$-I structure. The origin for the discrepancy between the LDOS and STM images for the $p(3\times2)$-I bilayer structure may be due to limitations in the employed tip model (e.g., the *s*-wave tip model) or due to strong tip-surface interactions. Note that the bias voltage of 0.1 V is low and is not expected to influence the contrast and STM-LDOS comparison. In fact, in our experiments the contrast does not depend on polarity of the applied bias voltage, within the voltage range of atomic resolution (-1.5–$+0.2$ V).

For the tri- and quadrolayers, our recorded atomically resolved STM images exhibit similar features as those of the bilayer, whereas thicker layers render a tip crash and cannot be imaged. From the calculated LDOS for the trilayer (not shown), we also observe similar features as for the bilayer, but without the pairing of the protrusions. The interpretation for the tri- and quadrolayer STM images is thus similar as for the mono- and bilayers, that is, only Cl^- ions are imaged as protrusions. Note that the small apparent heights of the tri- and quadrolayers result in a short tip-surface distance, which may affect the imaging.[26] In order to realistically model STM images of layers thicker than a bilayer it might be necessary to include a realistic tip model and a proper treatment of tip-surface interactions.

The apparent heights Δz_l of the single steps on the NaCl multilayer l provide indirect information about the conductance through the layers. For example, Δz_l is equal to zero and equal to the geometrical height for a multilayer l of vacuum and Cu, respectively. Because bulk NaCl is a wide-gap insulator with a band gap of 8.5 eV,[27] the electrons around the Fermi level have to tunnel through the film; therefore the insulating properties of the overlayer is manifested in a smaller apparent height than that of the geometrical height.

As shown in Table I, the calculated Δz_l are in good agreement with the experimentally measured Δz_l for the mono- and bilayers and are indeed appreciably smaller than the geometrical heights. In particular, we find that an adsorbed multilayer corresponds to a vacuum layer with a height of about half the geometrical height of the multilayer. The increasing difference in geometrical height and apparent heights with the number of layers makes it increasingly difficult to image the layer. The larger Δz_1 than Δz_l for $l>1$ is consistent with the behavior of the calculated partial *s*, *p*, and *d* DOS around the Cl^- ions, as shown in Fig. 7. The interface layer has the largest conductivity because of the formation of a weak covalent bond between a Cl^- ion in the interface layer and the Cu substrate results in a nonvanishing density of states in the gap region in the interface layer, whereas for the other layers, this contribution to the density of states are vanishingly small, resulting in a smaller conductance and smaller apparent heights than for the interface layer. Note that the variation of the work functions with the number of adsorbed layers contributes to Δz_l but cannot explain the variation in Δz_l with l. For instance, the decrease of the work function from the monolayer to the bilayer reduces the difference between Δz_1 and Δz_2 because the wave functions for electrons at the Fermi level decreases more slowly with decreasing work function.

Finally, the measured dI/dV spectrum also revealed how the tunneling through a NaCl overlayer is affected by the presence of a band gap in bulk NaCl. The characteristic features of this spectrum such as the strong reduction of dI/dV for voltages in the range from -4.5 to 2 V is reproduced rather well by the simulated dI/dV spectrum. This drastic reduction suggests a depletion of the LDOS in the corresponding energy region, which can be attributed to the absence of propagating states in the overlayer in this energy region and the formation of a band gap. However, our discussion in Sec. III of the simulated dI/dV spectrum in Fig. 8 showed that this suggestion is an oversimplification. The onset at around $V=2$ V is an LDOS effect whereas the onset at $V=-4.5$ V is caused by the voltage-dependent barrier and field emission.[28]

V. CONCLUSIONS

In conclusion, we have carried out a combined STM and density-functional study of the surface topography, the apparent height, work function, and differential conductance of mono-, bi-, and trilayers of NaCl on a stepped Cu(311) surface. The experimental results are well reproduced by the calculations, which also provide physical insights and an interpretation of the results. The adsorption-induced changes of electronic and geometric structure of the NaCl overlayer are found to be significant. The observed large adsorption-induced changes in the work function are found to be associated with substantial charge rearrangements upon adsorption. The Cl^- ions were shown to be imaged as protrusions. In the STM images, also the different positions of the Cl^- ions relative to the underlying Cu(311) lattice in the $p(3\times2)$-I and $p(3\times2)$-II structures of the NaCl monolayer were resolved. The poor conductivity of the layers were revealed by the fact that the apparent heights of steps were only half of the geometrical heights. Furthermore, dI/dV spectra revealed a large reduction of the tunneling conductance in a large voltage range, resembling a band gap. However, the simulated spectrum showed that only the onset at positive sample voltages may be viewed as a conduction-band edge, whereas the onset at negative voltages is due to the drastic effect the electric field from the tip has on the tunneling barrier.

ACKNOWLEDGMENTS

We gratefully acknowledge partial funding by the EU-RTN project "AMMIST." F.O. and M.P. are grateful for support from the Swedish Research Council (VR) and the Swedish Foundation for Strategic Research (SSF) through the materials consortium "ATOMICS." Allocations of computer resources through the Swedish National Allocations Committee (SNAC) and the Consortium of Heavy Computing (KTB) at Chalmers are also gratefully acknowledged.

[1] W. Hebenstreit, J. Redinger, Z. Horozova, M. Schmid, R. Podlucky, and P. Varga, Surf. Sci. **424**, L321 (1999).
[2] S. Schintke, S. Messerli, M. Pivetta, F. Patthey, L. Libioulle, M. Stengel, A. DeVita, and W. D. Schneider, Phys. Rev. Lett. **87**, 276801 (2001).
[3] J. Libuda, F. Winkelmann, M. Bäumer, H. J. Freund, T. Bertams, N. Neddermeyer, and K. Müller, Surf. Sci. **318**, 61 (1994).
[4] M. Bäumer and H. J. Freund, Prog. Surf. Sci. **61**, 127 (1999).
[5] J. Repp, S. Fölsch, G. Meyer, and K.-H. Rieder, Phys. Rev. Lett. **86**, 252 (2001).
[6] F. E. Olsson and M. Persson, Surf. Sci. **540**, 172 (2003).
[7] J. Tersoff and D. R. Hamann, Phys. Rev. Lett. **50**, 1998 (1983).
[8] K. Glöckler, M. Sokolowski, A. Soukopp, and E. Umbach, Phys. Rev. B **54**, 7705 (1996).
[9] G. Meyer, Rev. Sci. Instrum. **67**, 2960 (1996).
[10] Note that a proper notation of the overlayer with respect to the Cu(311) lattice can be phrased in matrix notation as (0 3; 1 1) for both structures (Ref. 29).
[11] G. Binnig, H. Rohrer, Ch. Gerber, and E. Weibel, Phys. Rev. Lett. **49**, 57 (1982).
[12] N. D. Lang, Phys. Rev. B **37**, 10 395 (1988).
[13] L. Olesen, M. Brandbyge, M. R. Sørensen, K. W. Jacobsen, E. Lægsgaard, I. Stensgaard, and F. Besenbacher, Phys. Rev. Lett. **76**, 1485 (1996).
[14] R. Bennewitz, M. Bammerlin, M. Guggisberg, C. Loppacher, A. Baratoff, E. Meyer, and H.-J. Günterrodt, Surf. Interface Anal. **27**, 462 (1999).
[15] G. Kresse and D. Joubert, Phys. Rev. B **59**, 1758 (1999).
[16] P. E. Blöchl, Phys. Rev. B **50**, 17 953 (1994).
[17] G. Kresse and J. Furthmüller, Phys. Rev. B **54**, 11 169 (1996).
[18] J. P. Perdew, J. A. Chevary, S. H. Vosko, K. A. Jackson, M. R. Pederson, D. J. Singh, and C. Fiolhais, Phys. Rev. B **46**, 6671 (1992).
[19] The slab contained six layers of Cu atoms. We used the same slab for the mono- and bilayers, where a vacuum region corresponding to 17 Å for the bare Cu slab was used. For the trilayer, the vacuum region corresponded to 25 Å for the bare Cu slab. The surface unit cell contained three Cu atoms in each substrate layer and two Na^+ and Cl^- ions in each NaCl layer. The surface Brillouin zone (SBZ) was sampled using 36 *k* points and the plane-wave cutoff energy was 300 eV.
[20] The atomic positions of the Na^+ and Cl^- ions and the first two layers of the Cu slab were allowed to relax, whereas the remaining four Cu layers were fixed at their bulk equilibrium positions.
[21] L. Bengtsson, Phys. Rev. B **59**, 12 301 (1999).
[22] J. Neugebauer and M. Scheffler, Phys. Rev. B **46**, 16 067 (1992).
[23] F. E. Olsson, N. Lorente, M. Persson, L. J. Lauhon, and W. Ho, J. Phys. Chem. B **106**, 8161 (2002).
[24] N. D. Lang, Phys. Rev. B **34**, 5947 (1986).
[25] C. J. Chen, Phys. Rev. B **42**, 8841 (1990).
[26] W. A. Hofer, A. J. Fisher, R. A. Wolkow, and P. Grütter, Phys. Rev. Lett. **87**, 236104 (2001).
[27] The experimentally measured band gap for bulk NaCl is 8.5 eV (Ref. 30), whereas the calculated band gap is 5.0 eV.
[28] Ultraviolet photoemission and electron energy-loss spectroscopy measurements by S. Fölsch (Ph. D. thesis, Hannover University, 1991) showed a fully developed band gap of about 8.5 eV already for a NaCl bilayer on Ge(100).
[29] M. C. Desjonquéres and D. Spanjaard, *Concepts in Surface Physics* (Springer-Verlag, Berlin, 1996).
[30] R. T. Poole, J. G. Jenkin, J. Liesegang, and R. C. G. Leckey, Phys. Rev. B **11**, 5179 (1975).